Advances in Computer, Signals and Systems (2025)
Clausius Scientific Press, Canada

DOI: 10.23977/acss.2025.090301
ISSN 2371-8838 Vol. 9 Num. 3

Two Filters Based on Simple Functions for Extracting Profiles from Images

Junshu Wu[1,a], Ye Wu[2,b,*]

[1]*Shenzhen Foreign Languages School, Longhua, Shenzhen, 518131, China*
[2]*School of Electrical and Automation Engineering, Nanjing Normal University, Nanjing, 210046, China*
[a]*75733145@qq.com*, [b]*chemwuye@njnu.edu.cn*
**Corresponding author*

Keywords: Low-Light Images, Gabor Filter, Graphical Contour Extraction, Fluorescence Microscope, Fluorescence Imaging

Abstract: Graphic contour extraction is a significant issue in pattern recognition and vision processing. However, classical filters such as Sobel filters are difficult to extract the complete shapes in terms of contour extraction. In this work, we designed two filters via logarithmic, sine, exponential, and cosine functions. These filters can extract the outline of the image completely. Moreover, a low-light image acquired from a fluorescence microscope was used for contour extraction. These filters could be used for extracting some of the edge contours for images with weak fluorescence and underwater images, where colouring impact was applied to the outputting images for generating coloured images. Meanwhile, the successful extraction of crystal contours under the fluorescence microscope via these filters proved their feasibility for microscopic image processing.

1. Introduction

In the field of vision, shape is the most intuitive feature of a figure. The current target recognition methods can be classified as area feature-based target recognition and contour feature-based target recognition methods. Target recognition based on contours is more logical, more stable, and less susceptible to interfering issues as compared to regional cues like colour and texture. As a result, contour feature recognition has wider application in many fields such as industry, medical, and mapping. As the basis of contour feature recognition, contour extraction has been the object of research by many scholars. To some extent, the goodness of the contour extraction method directly affects the subsequent contour feature recognition.

The traditional contour extraction methods such as Roberts operator, Prewitt operator, Canny operator, and LoG operator, which belong to the edge detection via differential operator. Their core idea is to segment the image contour with the image grey mutation as the boundary to further extract the graphic contour. With the continuous development of graphics processing technology, the requirements for graphic contour accuracy extraction have been gradually improved, and scholars have conducted more in-depth research. For example, some scholars have proposed SUSAN-based edge detection method. This method was used to study the size and second-order moments of similar

regions of image kernels to obtain the edge position of the image, but the algorithm requires artificially determined thresholds and has a large amount of operations [1]. In addition, with the continuous development of deep learning, some scholars use neural networks for image processing [2-8]. For example, some scholars built a holistic nested edge detection method with multi-scale and multi-feature learning, which adopts a global processing method and can automatically arrange and combine the scale information to obtain the optimal contour information of the image [9]. Some scholars proposed wavelet transform-based edge detection algorithm, which determines the boundary of an image by obtaining the local maximum of the wavelet coefficient amplitude after wavelet transform, and achieves a good detection effect, but it is easy to cause the detected image edge to be discontinuous or generate pseudo-edge [10]. It can be found that wavelets can be used to explore subjects with interrupted features in order to meet the purpose of spatial filtering [11-14]. We can construct a unique framework to filter the frequencies brought by the wavelet transform through the combination of functions to achieve the continuity of the extracted graphic contours. We have found two frameworks that are based on the combination of logarithmic and cosine functions and exponential and sine functions, respectively. Based on these frameworks, we have developed two filters dubbed as log-cos and exp-sin for contour extraction.

In Sec. 2 we presented two kinds of frameworks for constructing mathematical function-based filters. We showed the performance of these filters in Sec. 3 when processing simple picture, a weak-light image, an image obtained from a fluorescence microscope, and images acquired underwater. It can be seen that much more details can be acquired from these filters. This fully demonstrates the excellent ability of these filters to extract graphics contours.

2. Method

Algorithm 1: The log-cos filter

1) Reading the image in JPG format.
2) Converting the image into a grey image.
3) The image is resized to be 1440×2560.
4) Calculating wavelet transform using the pixels value and getting the coefficient value of v(m, n).
5) Calculating the new coefficient value $u_5(m, n)$using the following equations：

$$u_1(m,n) = a_1 \times hybot[u(m,n), a_2 \times u(m,n)]$$

$$u_2(m,n) = 2 \times log[a_3 \times u_1(m,n) + a_4] + \{3 \times log[a_5 \times u_1(m,n) + a_6]\}^2 + \{4 \times log[a_7 \times u_1(m,n) + a_8]\}^3 + \{5 \times log[a_9 \times u_1(m,n) + a_{10}]\}^4$$

$$u_3(m,n) = [a_{11} \times u_2(m,n)]^{a_{12}}$$

$$u_4(m,n) = a_{13} \times cos[a_{14} \times u_3(m,n)] + a_{15} \times cos[a_{16} \times u_3(m,n)] + a_{17} \times cos[a_{18} \times u_3(m,n)]$$

$$u_5(m,n) = \frac{u_3(m,n)}{cos[u_4(m,n)+a_{19}]}$$

6) Calculating the inverse of wavelet transform using the value of $u_5(m,n)$ and getting the new pixels values of $x(m,n)$.
7) Showing the processed image using the value of $x(m,n)$.

Algorithm 2: The exp-sin filter

1) Reading the image in JPG format.
2) Converting the image into a grey image.
3) The image is resized to 1440×2560.
4) Calculating wavelet transform using the pixels value and getting the coefficient value of $v(m,n)$.
5) Calculating the new coefficient value $v_5(m,n)$ using the following equations：

$$v_1(m,n) = b_1 \times hypot[v(m,n), b_2 \times v(m,n)]$$

$$v_2(m,n) = e^{b_3 \times v_1(m,n) + b_4}$$

$$v_3(m,n) = [b_5 \times v_2(m,n)]^{b_6}$$

$$v_4(m,n) = b_7 \times sin[b_8 \times v_3(m,n)] + b_9 \times sin[b_{10} \times v_3(m,n)] + b_{11} \times sin[b_{12} \times v_3(m,n)] + b_{13} \times sin[b_{14} \times v_3(m,n)]$$

$$v_5(m,n) = \frac{v_3(m,n)}{cos[v_4(m,n)+b_{15}]}$$

6) Calculating the inverse of wavelet transform using the value of $v_5(m,n)$ and getting the new pixels values of y(m,n).
7) Showing the processed image using the value of $y(m,n)$.

We built two filters, which are named as log-cos filter and exp-sin filter. They are built based on the wavelet transform and the simple functions. In order to get the log-cos filter, we have used the logarithmic and cosine functions along with a general wavelet decomposition using typical function of Symlets. In addition, we created the exp-sin filter based on the exponential and sine functions, which decomposes the image into waves after grayscale and pixel processing. Here we use the sym4 function for the wavelet decomposition. From this we can obtain the coefficient value v(m, n) of the wavelet decomposition. After a series of function processing, we can get a new coefficient value v5 (m,n). We obtained the outputting image using the coefficient of v5 (m,n). The frameworks for these two filters are shown as follows.

3. Results and discussion

3.1. Extracting the profiles of simple shapes

In order to verify the effectiveness of these two filters for extracting edge contours, we chose a graph with nested structures for processing. Fig. 1a shows an image named as Multi. Fig. 1b shows the outputting image after log-cos filtering. Fig. 1c shows the image obtained after the exp-sin filter processing of this picture. The image after the processing of using the filters shows the detailed contours of the inner and outer nested graphs more clearly. Fig. 1d shows the outputting image of Multi via the Sobel filter. The inner nested triangles are not extracted at all in the image processed by the Sobel filter.

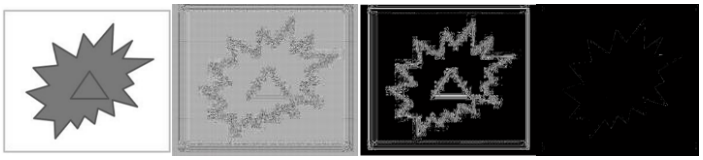

(a) (b) (c) (d)

Figure 1: (a) An image called as Multi. (b) Processed by the log-cos filter. (c) Processed by the exp-sin filter. (d)Processed by Sobel operator.

By comparing the processing results of Fig. 1a, it can be seen that the log-cos filter and the exp-sin filter can extract the inner nested graphs clearly and completely compared to the Sobel filter.

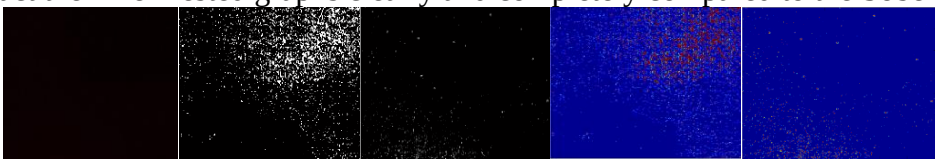

(a) (b) (c) (d) (e)

Figure 2: (a) A weak-light image called as Fungal was acquired from a fluorescence microscope. (b) Processed by combing a wavelet-based filter and the log-cos filter. (c) Processed by combing a wavelet-based filter and the exp-sin filter. (d) Colouring with the log-cos filter. (e) Colouring with the exp-sin filter.

3.2 Combing with the wavelet filter

We combine our filters with a wavelet filter for extracting the contours from a weak-light image. Here, a weak-light image denoted as Fungal (Fig.2a) was first processed by the wavelet filter designed by Man Jia et al [15]. This would generate the outputting image A1, which was further processed by the log-cos filter and the exp-sin filter. The outputting images from these filters were shown in Fig. 2b and Fig. 2c, respectively.

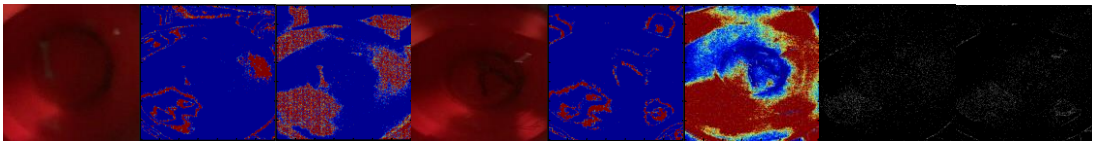

(a) (b) (c) (d) (e) (f) (g) (h)

(a) Input image Water21. (b) The image Water21 was processed by combing a wavelet-based filter and the log-cos filter. (c) The image Water21 was processed by combing a wavelet-based filter and the exp-sin filter. (d) Input image Water22. (e) The image Water22 was processed by combing a wavelet-based filter and the log-cos filter. (f) The image Water22 was processed by combing a wavelet-based filter and the exp-sin filter. (g) The image Water21 was processed by Sobel operator. (h) The image Water22 was processed by Sobel operator.

Figure 3: Sample images acquired under water were processed.

The parameter of measurement of the entropy was used to evaluate the processing impact of these filters [15]. The values of measurement of the entropy for the image Fig. 2b and Fig. 2c were calculated as 1.3722 and 0.2018, respectively. The outputting images of our filters are grey, which may be not vivid for presentation. Therefore, we used colouring strategy for introducing the coloured output. Fig. 2d and Fig. 2e are the coloured images corresponding to the images of Fig. 2b and Fig. 2c.

People have placed much attention to the underwater observation and utilization of marine resources. Underwater image processing becomes an active research field. It should be noted that marine environment is usually faced with complex conditions, including water turbulence, wave diffusion, light absorption and scattering, and noises from sea animals. This is different from the ordinary environment. Therefore, the images acquired may show the features of low contrast, uniform light irradiation, and colour distortion. All these imaging environment has made the extraction of the profiles from the images acquired from the underwater condition a difficult task. Here, we tried to process the underwater images using the framework of the wavelet-based filter [15] combined with the log-cos filter or the exp-sin filter. Fig.3a is an image acquired from underwater condition. Fig.3b and Fig.3c were the output images generated by combing the wavelet-based filter and the log-cos filter or the exp-sin filter. The values of the entropy for the image Fig. 3b and Fig.3c were calculated as 0.7456 and 2.5680. Fig.3d is another image acquired underwater condition. Fig.3e and Fig.3f were the output images generated by combing the wavelet-based filter and the log-cos filter or the exp-sin filter. The values of the entropy for the image Fig. 3e and Fig.3f were calculated as 0.4322 and 11.9625. Fig.3g and Fig.3h showed the output images generated by Sobel operator. Clearly, there were missing features in Fig.3g and Fig.3h. Those key features of the wrench and the pincer were shown in Fig.3b, Fig.3c, Fig.3e, and Fig.3f.

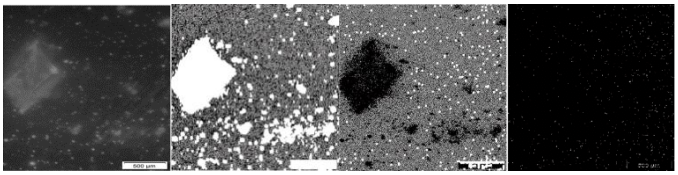

(a) (b) (c) (d)

Figure 4: (a) A sample image called as Crystal and its processed versions, including those (b) processed by the log-cos filter, (c) processed by the exp-sin filter (d) processed by Sobel operator.

In addition, we further explored the effect of these two filters on the extraction of edge contours from images taken under fluorescence microscopy. Fig. 4a shows a picture named Crystal taken under fluorescence microscope. Fig. 4b, Fig. 4c, and Fig. 4d show the pictures processed by the log-cos filter, the exp-sin filter, and Sobel operator, respectively. We can see that the log-cos filter and the exp-sin filter have clearer graphic details than the original images taken under the fluorescence

microscope. It fully demonstrates the distribution of all the features, which can be more convenient for researchers to process and study the crystal materials. It can be seen that the images processed by the Sobel operator have a loss of detail contours compared to the original unprocessed images.

Through the above comparative study, we can see that the filters built has a much better graphic contour extraction ability compared with the Sobel operator. What is more rare is that there are various combinations of functions in the framework, where our proposed scheme is based on such an adjustable framework. Therefore, we can say that there is still much to explore and discover in this aspect. At the same time, they can show the anti-interference and the good applicability for the extraction of graphic contours under fluorescence microscopy. We can change this dynamic framework to achieve better image contour extraction capability in our work. It can be expected that they can be modified to meet the needs of a wider range of industrial applications. It has been reported that Gabor filter [18], watershed algorithm based filter [19], and matched filter [20] are effective in processing images, where the combination of these filters with our designed filters can be expected to show a lot of practical applications.

It is reported that wavelets and lifting-wavelets can be used to create special filters for enhancing the low-light images [19-20], which may be integrated into our framework for getting patterns of the low-light images. Another aspect of the future work would be using advanced imaging technology and nanomaterials [21-25]. It can be noted that the images were enhanced after using the Retinex models and their derivatives [26-30]. This would be our future endeavour.

4. Conclusions

For graph contour extraction, we created two frameworks. One is based on the combination of the logarithmic and the cosine functions. Another is based on the combination of the exponential and the sine functions. These filters are more powerful than the Sobel filter for extracting the contours of complex graphs, where they can extract the nested graphs completely and clearly. In addition to this, we compared the image acquired from the fluorescence microscope and processed via the log-cos filter, the exp-sin filter, and Sobel filter. From the extracted images, we can see that the features of the crystals can be clearly seen in the images processed by our proposed two filters, while the images processed by Sobel filter cannot be extracted. Our proposed filter can bring convenience to future research in chemical and medical imaging.

Acknowledgements

We thank the technique support from the faculty of Nanjing Normal University.

References

[1] Smith S. M., De Stefano N., Jenkinson M. and Matthews, P.M. (2001) Normalized accurate measurement of longitudinal brain change. Journal of Computer Assisted Tomography, 25, 466-475.
[2] Wang B., Chen L. L. and Zhang Z. Y. (2018) A novel method on the edge detection of infrared image. Optik, 180, 610-614.
[3] Wang Z. –F., Yu Y. –F., Wang J., Zhang J.-Q., Zhu H.-L., Li P., Xu L., Jiang H.-N., Sui Q.-M., Jia L. and Chen J.-P.(2022) Convolutional neural-network-based automatic dam-surface seepage defect identification from thermograms collected from UAV-mounted thermal imaging camera. Construction and Building Materials, 323, 126416.
[4] Yang G., Wang B., Qiao S., Qu L., Han N., Yuan G., Li H., Wu T. and Peng Y. (2022) RETRACTED: Distilled and filtered deep neural networks for real-time object detection in edge computing. Neurocomputing, 505, 225-237.
[5] Cao J., Chen .L, Wang M. and Tian Y. (2018) Implementing a Parallel Image Edge Detection Algorithm Based on the Otsu-Canny Operator on the Hadoop Platform. Computational Intelligence and Neuroscience, 3598284.
[6] Tchinda B. S., Tchiotsop D., Noubom M., Louis-Dorr V. and Wolf D. (2021) Retinal blood vessels segmentation using classical edge detection filters and the neural network. Informatics in Medicine Unlocked, 100521.

[7] Kenning M., Deng J., Edwards M. and Xie X. (2022) A directed graph convolutional neural network for edge-structured signals in link-fault detection. Pattern Recognition Letters, 153, 100-106.
[8] Araghi L. F. and Arvan M. R. (2009) An implementation image edge and feature detection using neural network. Proceedings of the International Multi Conference of Engineers and Computer Scientists 2009 Vol I , IMECS 2009, March 18 - 20, 2009, Hong Kong, China.
[9] Xie S. and Tu Z. (2015) Holistically-nested edge detection, Proceedings of the IEEE International Conference on Computer Vision (ICCV), Santiago: IEEE, 1395-1403.
[10] Sur A., Patra N., Chakraborty S. and Saha I. (2009) A new wavelet based edge detection technique for Iris imagery. IEEE International Advance Computing Conference, IACC2009, 2009, 120-124.
[11] Romani L., Rossini M. and Schenone D. (2019) Edge detection methods based on RBF interpolation. Journal of Computational and Applied Mathematics, 349, 532-547.
[12] Choi J.K., Dong B. and Zhang X. (2020) An edge driven wavelet frame model for image restoration. Applied and Computational Harmonic Analysis, 48,993-1029.
[13] Noras P. and Aghazadeh N. (2018) Directional schemes for edge detection based on B-spline wavelets. Circuits, Systems, and Signal Processing, 37, 3973-3994,
[14] Fu Z., Song S., Wang X., Li J. and Tai H.-M. (2018) Imaging the topology of grounding grids based on wavelet edge detection. IEEE Transactions on Magnetics, 54, 1-8.
[15] Jia M., Xu J., Yang R., Li Z., Zhang L. and Wu Y. (2023) Three filters for the enhancement of the images acquired from fluorescence microscope and weak-light-sources and the image compression. Heliyon, 9, e20191.
[16] Shen L. –L. and Ji Z. (2009) Gabor wavelet selection and SVM classification for object recognition. Acta Automatica Sinica, 35, 350-355.
[17] Bleau A. and Leon L. J. (2000) Watershed-Based Segmentation and Region Merging. Computer Vision and Image Understanding, 77, 317-370.
[18] Chaudhuri S., Chatterjee S., Katz N., Nelson M. and Goldbaum M. (1989) Detection of blood vessels in retinal images using two-dimensional matched filters. IEEE Transactions on Medical Imaging, 8, 263-269.
[19] Yang R., Chen L., Zhang L., Li Z., Lin Y. and Wu Y. (2023) Image enhancement via special functions and its application for near infrared imaging. Global Challenges, 2200179.
[20] Huang Y., Yang R., Geng X., Li Z. and Wu Y. (2023) Two filters for acquiring the profiles from images obtained from weak-light background, fluorescence microscope, transmission electron microscope, and near-infrared camera. Sensors, 23, 6207
[21] Zhu J., Shao X. –J., Li Z., Lin C.-H., Wang C.-W.-Q., Jiao K., Xu J., Pan H.-X. and Wu Y. (2022) Synthesis of Holmium-Oxide Nanoparticles for Near-Infrared Imaging and Dye-Photodegradation. Molecules, 27, 3522.
[22] Li Z., Li Y., Lin Y., Alam M. Z. and Wu Y. (2020) Synthesizing Ag+: MgS, Ag+ : Nb_2S_5, Sm^{3+}: Y_2S_3, Sm^{3+}:Er_2S_3 and Sm^{3+}:ZrS_2 compound nanoparticles for multicolor fluorescence imaging of bio-tissues. ACS Omega, 51, 32868–32876.
[23] Wu Y., Yang J., Lin Y. and Xu J. (2019) Synthesis of samarium-based metal organic compound nanoparticles with polychromatic-photoluminescence for bio-tissue fluorescence imaging. Molecules, 24, 3657.
[24] Wu Y., Lin Y. and Xu J. (2019) Synthesis of Ag-Ho, Ag-Sm, Ag-Zn, Ag-Cu, Ag-Cs, Ag-Zr, Ag-Er, Ag-Y and Ag-Co metal organic nanoparticles for UV-Vis-NIR wide-range bio-tissue imaging. Photochemical & photobiological sciences, 18, 1081-1091,
[25] Wu Y., Ou P., Song J., Zhang L., Lin Y., Song P. and Xu J. (2020) Synthesis of praseodymium-and molybdenum-sulfide nanoparticles for dye-photodegradation and near-infrared deep-tissue imaging, Materials Research Express, 7, 036203.
[26] Tang Q., Yang J., He X., Jia W., Zhang Q. and Liu H. (2021) Nighttime image dehazing based on Retinex and dark channel prior using Taylor series expansion. Computer Vision and Image Understanding, 202, 103086.
[27]Wang Y. and Zhang Z. (2023) Global attention retinex network for low light image enhancement. Journal of Visual Communication and Image Representation, 92,103795.
[28] Wang Y., Chen J., Han Y. and Miao D. (2022) Combining attention mechanism and Retinex model to enhance low-light images. Computers & Graphics, 104, 95-105.
[29] Cai R. and Chen Z. (2023) Brain-like retinex: A biologically plausible retinex algorithm for low light image enhancement. Pattern Recognition, 136, 109195.
[30] Zhang X. and He C. (2023) A robust structure and texture aware model for image Retinex. Applied Mathematical Modelling, 113, 206-219.